RSC Advances

PAPER

View Article Online
View Journal | View Issue

Cite this: *RSC Adv.*, 2020, **10**, 24642

CO_2 and water vapor adsorption properties of framework hybrid W-ZSM-5/silicalite-1 prepared from RHA

Yisong Wang, He Jia, Xin Fang, Ziyang Qiu and Tao Du *

Framework hybrid W-ZSM-5 and W-silicalite-1 zeolites were synthesized by hydrothermal methods using rice husk ash (RHA) as a silicon raw material. RHA is a low-cost precursor material, and its use can also alleviate the environmental and human health related problems that may occur when it is stacked in open fields. A series of comparative samples were characterized by XRD, FTIR, ICP-OES, SEM, N_2 adsorption–desorption and pore size analysis in order to examine their crystal structure, hybrid state, morphology and textural properties. The maximum CO_2 adsorption capacities of W-ZSM-5 and W-silicalite-1 are 81.69 and 69.96 $cm^3\ g^{-1}$, respectively, measured at 15 bar. The isotherms of CO_2, N_2 and O_2 are perfectly fitted by the Toth model, and it is noted that the presence of Al atoms increases the heterogeneity. It can be seen that the greater the heterogeneity of the adsorbent, the larger the CO_2 adsorption capacity achieved. The incorporation of tungsten into the framework does not affect the crystallization of the zeolite, but it prevents the formation of silanol and O–H groups at the adsorption sites. Therefore, the CO_2/H_2O selectivity of W-ZSM-5 is slightly higher than that of ZSM-5, and that of W-silicalite-1 is three times that of silicalite-1. W-ZSM-5/silicalite-1 are promising adsorbents for separating CO_2 under humid industrial conditions.

Received 26th April 2020
Accepted 3rd June 2020

DOI: 10.1039/d0ra03736b

rsc.li/rsc-advances

1. Introduction

As the main greenhouse gas, carbon dioxide (CO_2) from factories is emitted into the atmosphere, contributing to the greenhouse effect and a series of problems for ecosystems, biodiversity and human economic activity.[1,2] In the short term, if there is no revolutionary development of new energy and energy storage technologies, fossil fuel combustion will still be needed to meet the growing demand for energy consumption.[3] A promising medium-term solution is carbon capture and utilization (CCU), which continuously captures CO_2 from industrial processes and converts it into value-added chemicals.[4] This technology is not enough to replace large-scale storage facilities for CO_2, but other economic chemical products can compensate for the cost of carbon emission reduction. The crucial technology captures CO_2 gas from power plants, industry and transportation.[5] In addition, CO_2 capture and separation technology is also used for air prepurification, natural gas purification and carbon removal from flue gas.[6–9] Aqueous amine absorption, solid adsorbent adsorption, membrane separation and cryogenic separation methods for CO_2 capture have received wide attention due to their respective advantages.[10–12] Instead of the aqueous alkanolamine absorbents, the use of solid adsorbents can avoid large amounts of renewable energy and equipment corrosion. They can also be used in pressure swing adsorption and temperature swing adsorption processes to separate CO_2 efficiently.[13] Hence, it is necessary to explore solid adsorbents that are superior in performance, economical to produce, and suitable for practical industrial conditions.

Zeolites are pore-rich solid adsorbents with regions of electric field due to their inherently negatively charged frameworks and cations. And thus they have unique physical adsorption properties. Yan *et al.* prepared amidoxime modified zeolite X to simulate its sensitivity change as a cerium ion adsorbent for industrial wastewater treatment.[14] Wanigarathna *et al.* optimized the pore size of zeolite 5A by chemical modification with tetraethyl orthosilicate to obtain pure R134a from a refrigerant mixture.[15] Zukal *et al.* prepared isoreticular siliceous zeolites for the separation of CO_2 and investigated the effect of their dimensions on the heat of adsorption.[16] Industrial waste, agricultural waste and natural minerals can be used as alternative synthetic raw materials for silicon and aluminum to improve the economics of preparation and facilitate large-scale application. The agricultural waste rice husk ash (RHA) contains more than 90% amorphous silica, which is suitable for preparing silica-based adsorbents including zeolites. Setthaya *et al.* synthesized a TiO_2–zeolite photocatalyst by a hydrothermal method with metakaolin and rice husk ash, which showed excellent performance in the adsorption and

State Environmental Protection Key Laboratory of Eco-Industry, Northeastern University, Shenyang 110819, China. E-mail: wangys@smm.neu.edu.cn; dut@smm.neu.edu.cn

degradation of methylene blue.[17] Khoshbin *et al.* synthesized a series of ZSM-5 zeolites using ultrasonic energy and studied their activity in the catalytic cracking of light naphtha.[18] Jesudoss *et al.* successfully synthesized ZSM-5 by a hydrothermal method using waste such as rice hull ash, and studied the potential cytotoxic effects of different concentrations of graded ZSM-5 zeolite on human lung epithelial carcinoma A549 cells.[19] RHA is a potential source of low-cost precursors, and its use can also alleviate the environmental and human health related issues that may occur when it is stacked in open spaces.[20] Further, the RHA concentrated in biomass power plants has excellent sustainability performance in environmental, economic and social assessments.[21]

The synthesis of ZSM-5 zeolite needs a template as a structure-directing agent, so it is easier to prepare it with inexpensive alternative raw materials.[22] In general, ZSM-5 zeolite with a low silicon/aluminum ratio has an excellent performance in pressure swing adsorption (PSA) applications, because the counter ions outside the framework are the main active adsorption sites for CO_2 adsorption.[23] Also, highly crystalline ZSM-5 with high surface area and adjustable three-dimensional pore structure is expected to become a promising CO_2 adsorbent.[24] Although ZSM-5 zeolite has been widely used and intensively explored in various fields, it also needs to be modified to improve the practicability for CO_2 adsorption; for example, hybrid zeolites doped with other substances have been prepared. Kalantarifard *et al.* synthesized ZSM-5 with large pore surface structures and modified it with ethylenediamine to achieve high CO_2 adsorption capacity from the gas stream.[25] Lin *et al.* used an amine bifunctional compounding strategy for the manufacture of a graft impregnated ZSM-5/KIT-6 composite, which exhibited excellent CO_2 adsorption performance and prospects for capturing CO_2 from actual flue gas.[26] It is well known that the CO_2 adsorption performance of adsorbents is largely influenced by water vapor in various industrial applications. Datta *et al.* prepared a microporous coppersilicate in which copper atoms were introduced into the framework of a titanosilicate in place of titanium atoms and achieved excellent CO_2 capture performance in humid flue gases and humid atmosphere.[27] Ke *et al.* used a bulky alkali metal–crown ether complex as a template to incorporate boron and copper heteroatoms into the framework of a high silicon RHO zeolite, which was used to remove traces of carbon dioxide from a CO_2/CH_4/N_2 mixture under humid conditions.[28] Ding *et al.* studied a method for liquid-phase oxidation of ethylamine with hydrogen peroxide on a tungsten-doped MOR zeolite, and the catalytic reaction activity was increased due to the change in the coordination state of the W species.[29] However, research on the incorporation of other atoms into the ZSM-5 framework has rarely been reported. Moreover, it is valuable to explore the effect of mixed atoms in the ZSM-5 framework on the adsorption of CO_2 and water vapor.

The aim of this work is to synthesize W-ZSM-5 and W-silicalite-1, in which tungsten is incorporated within the framework, using RHA as an alternative silicon raw material to reduce the cost of preparation. The physicochemical properties of the materials were investigated by means of characterization, and a series of CO_2, N_2, O_2 and water vapor adsorption measurements were performed. By comparing the experimental results with those for ZSM-5 and silicalite-1, the tungsten and aluminum content in the framework and its effect on gas adsorption were explored. Through calculation of the equilibrium adsorption amount, selectivity and water vapor adsorption properties, the materials were evaluated under actual humid multi-component industrial conditions.

2. Experimental

2.1. Materials

Fresh rice husk was obtained from local farms. The silica was then extracted from the RHA using alkali dissolution and acid leaching processes according to our previous work.[30] Hydrochloric acid (HCl), sodium aluminate ($NaAlO_2$), sodium tungstate dihydrate ($Na_2WO_4 \cdot 2H_2O$), sodium hydroxide (NaOH) and tetrapropylammonium hydroxide (TPAOH, 25 wt% in H_2O) were obtained from Sinopharm Chemical Reagent Co., Ltd. The helium, nitrogen, carbon dioxide and oxygen gas (all 99.999%) used in this work were supplied by Shenyang Shuntai Special Gas.

2.2. Preparation of W-ZSM-5/silicalite-1

W-ZSM-5 zeolite was synthesized by using a hydrothermal template method with an initial gel composition of $1.24Na_2O : 100SiO_2 : Al_2O_3 : 2WO_3 : 32TPAOH : 2000H_2O$. In a typical synthesis process, 0.032 g of NaOH and 0.27 g of $NaAlO_2$ were dissolved in 27 mL of deionized water, followed by the addition of 1.1 g of $NaWO_4 \cdot 2H_2O$ with continued stirring. After the stirred solution became clear, 43.4 g TPAOH and 10 g RHA silica were slowly added. Then, the solution was aged for 4 h at room temperature. The resulting mixed gel was transferred to a 200 mL Teflon-lined stainless-steel autoclave and sealed. The crystallization process was carried out in an oven at 165 °C for 48 h. The product was filtered, washed and completely dried, and finally calcined at 500 °C for 6 h in N_2 flow to remove the organic template. The Al-free zeolite W-silicalite-1 was synthesized similarly using the above chemical ratio and process, but without the addition of an Al source. As comparative samples, non-framework hybrid zeolites without tungsten were also synthesized, and named ZSM-5 and silicalite-1.

2.3. Characterization methods

The powder X-ray diffraction (XRD) data was collected on an XRD-7000S powder diffractometer (Shimadzu, Japan) with Cu Kα radiation ($\lambda = 0.154$ nm) operated at 40 kV and 40 mA. The samples were placed in a glass sample holder and scanned from $2\theta = 5$ to 40° with step size of 0.02° and scanning rate of 2° min^{-1}. The Fourier transform infrared (FTIR) spectra of the samples were recorded using a Cary 660 Spectrum One FTIR spectrometer (Agilent Technologies, Australia) within the wavenumber range of 3600–400 cm^{-1}. Before this, the samples were dried under vacuum for 2 h at 100 °C to avoid signal interference from adsorbed water. The inductively coupled plasma optical emission spectrometry (ICP-OES) analysis was

performed on an Optima 8300DV spectrometer (PerkinElmer, America) to determinate the element contents. Scanning electron microscopy (SEM) images were obtained on an ULTRA PLUS microscope (ZEISS, Germany) with a working distance of 8.7 mm at an accelerating voltage of 15 kV. The N_2 adsorption–desorption isotherm at −196 °C was measured with an ASAP 2020 adsorption instrument (Micromeritics, USA). Prior to the test, the samples were degassed at 350 °C for 5 h. The specific surface area, micropore volume, micropore distribution and mesoporous distribution were calculated by the Brunauer–Emmett–Teller (BET) method, t-plot method, Horvath–Kawazoe (HK) method and Barrett–Joyner–Halenda (BJH) method, respectively. The total pore volume was calculated at a relative pressure of $P/P_0 = 0.995$.

2.4. Adsorption measurements

CO_2, N_2 and O_2 gas adsorption capacity measurements were carried out on a 3H-2000PH adsorption instrument (BeiShiDe, China) with isotherms at −15, 0, 25 and 50 °C. The temperature was controlled by heating and cooling of the circulating glycol thermal fluid. The sample was pretreated at 350 °C for 5 h under a vacuum of 10^{-5} bar, and adsorption was carried out in a pressure range from approximately 0.01 to 15 bar. Water vapor adsorption–desorption isotherms were measured using a 3H-2000 PW gravimetric vapor adsorption instrument (BeiShiDe, China). During the test, the relative pressure was controlled at the target pressure through the volatilization of pure steam into the vacuum test chamber, and the temperature was constant at 25 °C. Before the sample was assembled, it was heated under the same conditions as above in order to remove moisture and impurities.

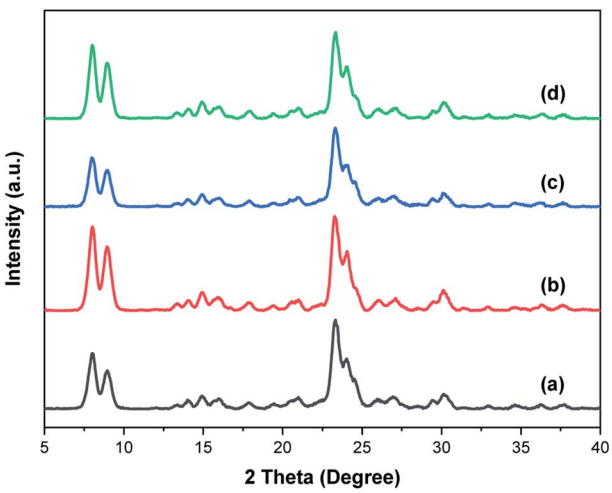

Fig. 1 XRD patterns of (a) W-ZSM-5, (b) W-silicalite-1, (c) ZSM-5 and (d) silicalite-1.

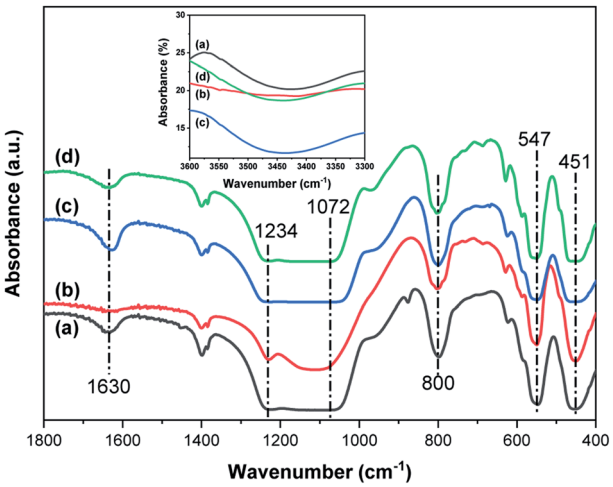

Fig. 2 FTIR spectra of (a) W-ZSM-5, (b) W-silicalite-1, (c) ZSM-5 and (d) silicalite-1.

3. Results and discussion

3.1. Characterization

Fig. 1 shows the XRD patterns of the synthesized zeolites W-ZSM-5, W-silicalite-1, ZSM-5 and silicalite-1. The MFI-type structure diffraction peaks at 7.8°, 8.9°, 23.5°, 23.7° and 24.1° are observed for all samples, and correspond to the (101), (200), (051), (033) and (133) crystal planes respectively.[31] This indicates that the incorporation of tungsten does not affect the zeolite framework type, and there are no diffraction peaks for Al_2O_3 or WO_3 crystals. For W-ZSM-5 and ZSM-5, the intensity of the peaks at $2\theta = 7$–9° is relatively low due to the Si/Al content ratio.[32] The unit cell parameters of the samples are listed in

Table 2 Elemental analysis from ICP-OES of the samples (at%)

Sample	Na	Si	Al	O	W
W-ZSM-5	0.21	42.76	0.72	55.62	0.68
W-silicalite-1	0.25	44.46	0.00	54.55	0.74
ZSM-5	0.18	41.73	0.92	57.16	0.00
Silicalite-1	0.05	42.63	0.00	57.32	0.00

Table 1 Unit cell parameters calculated from powder diffraction of the samples

Sample	Unit cell (Å)			Unit cell volume (Å^3)	Interplanar spacing (051)
	a	*b*	*c*		
W-ZSM-5	19.9895	19.8621	13.3258	5290.78	3.8069
W-silicalite-1	19.9264	19.8092	13.2528	5231.21	3.7959
ZSM-5	19.9927	19.8649	13.3040	5283.70	3.8068
Silicalite-1	19.8786	20.3437	13.2802	5370.56	3.8903

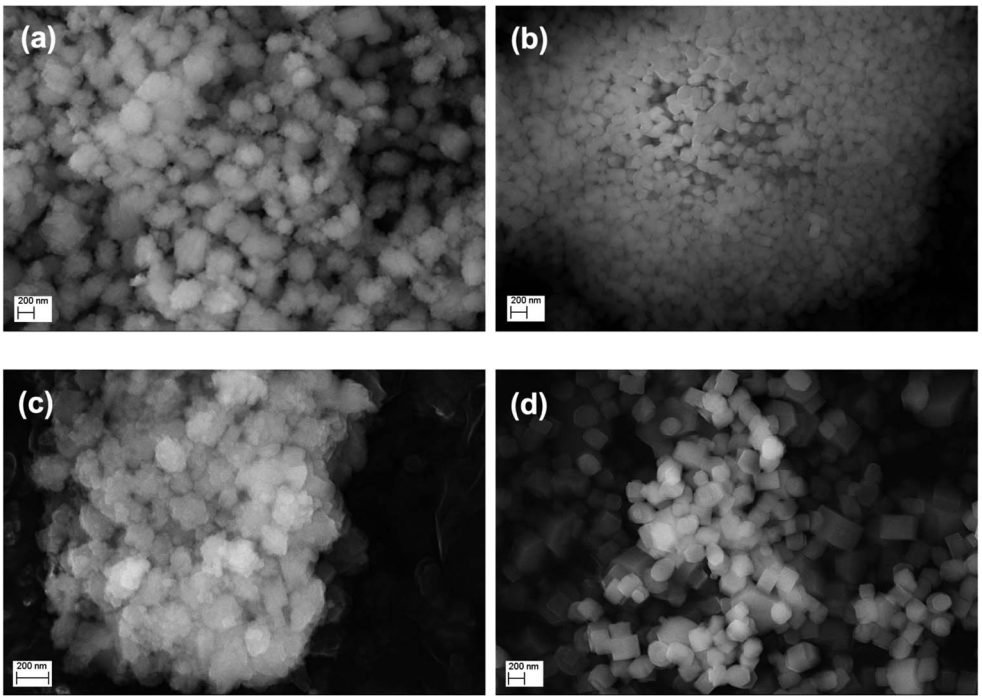

Fig. 3 SEM images of (a) W-ZSM-5, (b) W-silicalite-1, (c) ZSM-5 and (d) silicalite-1.

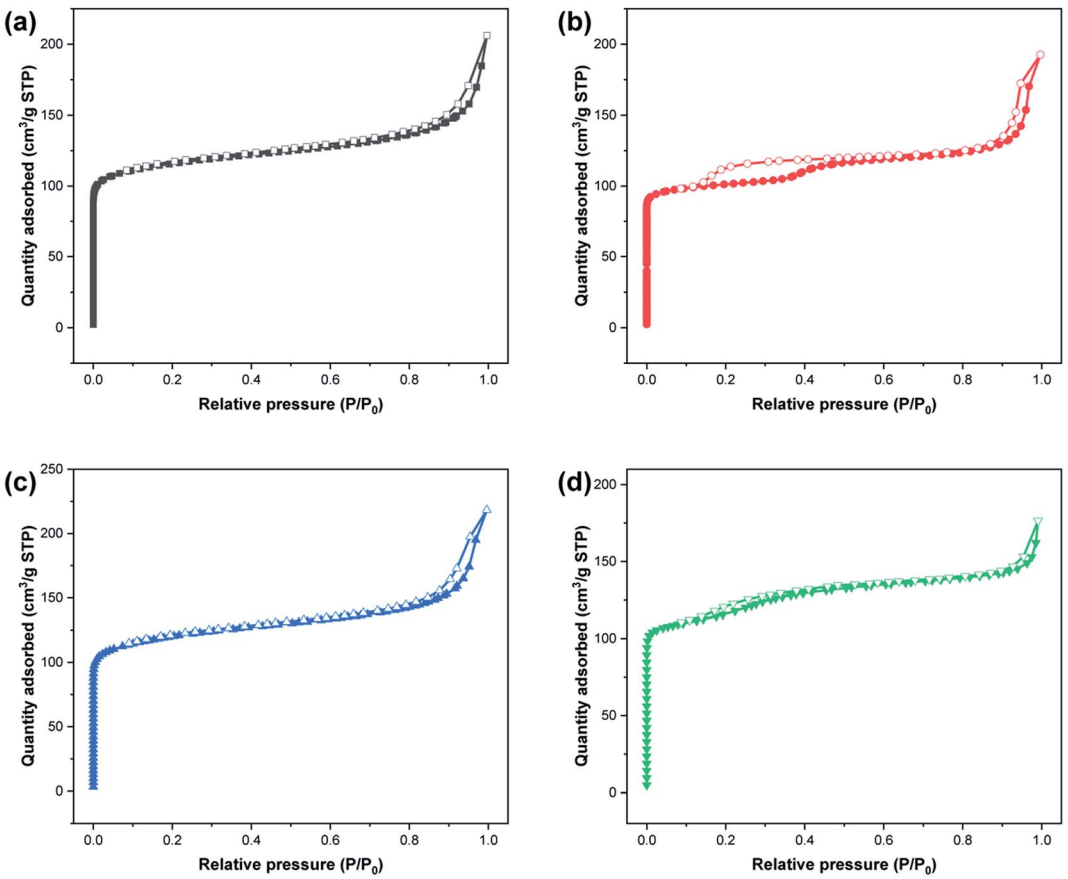

Fig. 4 N_2 adsorption–desorption isotherms of (a) W-ZSM-5, (b) W-silicalite-1, (c) ZSM-5 and (d) silicalite-1. Filled symbols: adsorption; empty symbols: desorption.

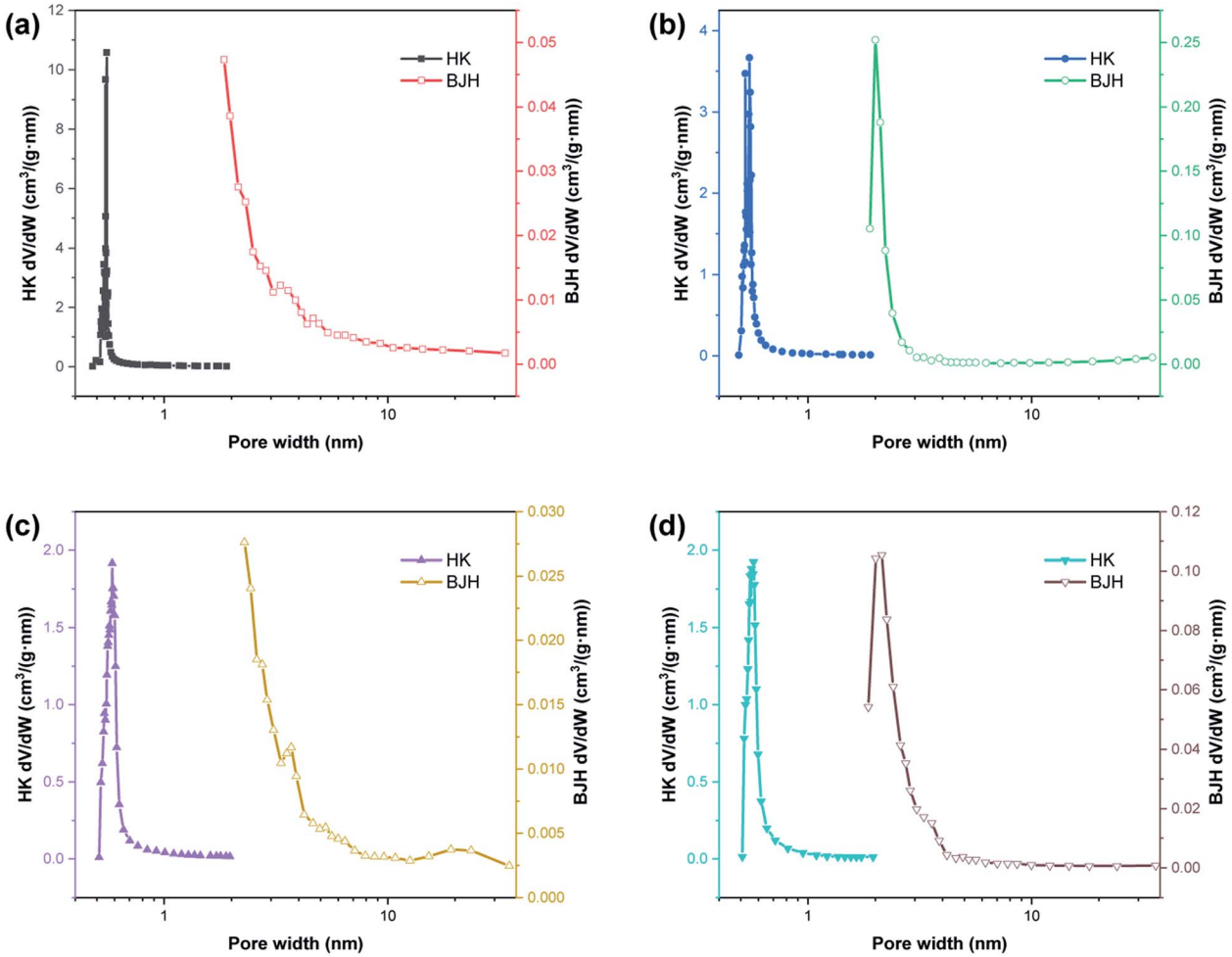

Fig. 5 HK and BJH pore size distributions of (a) W-ZSM-5, (b) W-silicalite-1, (c) ZSM-5 and (d) silicalite-1.

Table 1. The differences in the values of the unit cell volume and the interplanar spacing indicate that the zeolite framework contains a mixture of tungsten and aluminum atoms. Fig. 2 shows the FTIR spectra of the samples in the wavenumber ranges of 3600–3300 and 1800–400 cm^{-1}. The strong, broad bands at 1234 and 1072 cm^{-1} are due to the T–O stretching vibration and the asymmetric stretching vibration of the TO_4 tetrahedron, respectively (T = Si, Al, W). The bands at 800, 547, and 451 cm^{-1} are associated with the symmetric stretching vibrations of the tetrahedrons, typical vibrations connected to the outside of the tetrahedrons of the MFI framework structure, and Si–O bending vibrations, respectively. The bands at 3450 and 1630 cm^{-1} are ascribed to the OH stretching vibration of the silanol groups and the HOH bending vibration resulting from extended hydrogen bonding.[33–35] It can be clearly seen that the doping of tungsten atoms in the zeolite framework prevents the formation of silanol and O–H groups. The quantitative elemental analysis is summarized in Table 2. W atoms are present in the hybrid frameworks of W-ZSM-5 and W-silicalite-1, which is consistent with the XRD and FTIR findings. Fig. 3 shows SEM images of the microscopic appearance of the morphological features. The ZSM-5 type zeolite consists of agglomerated small particle crystals, and silicalite-1 consists of single angular crystals. The incorporation of tungsten has no effect on the appearance of the morphology, and only affects the internal framework. The crystal size of W-silicalite-1 is approximately 100 nm, compared with 200 nm for silicalite-1. Fig. 4 shows the N_2 adsorption–desorption isotherms at liquid nitrogen temperature, and the corresponding pore size distributions calculated by the HK and BJH models are shown in Fig. 5. The main difference in the isotherms is between the ZSM-5 and silicalite-1 types, in which a hysteresis loop is present for silicalite-1 due to the larger size of the mesopores. This may be due to reorientation of the nitrogen molecules, which increases the packing density and creates a more favorable quadrupole–quadrupole interaction. The step in the adsorption branch for W-silicalite-1 was located at higher P/P_0 compared to silicalite-1. The reason for the shift in this step is that W-silicalite-1 has 10% more mesopores than silicalite-1. The pore size properties of ZSM-5 are minimally affected by tungsten, but its influence on the BET surface area and mesopore ratio of silicalite-1 is not negligible. The detailed textural properties including surface area, pore volume and pore size are summarized in Table 3. It is seen that the presence or absence of Al atoms in the zeolite

Table 3 Textural properties of the prepared samples

Sample	S_{BET} (m^2 g^{-1})	V_{total} (cm^3 g^{-1})	V_{micro} (cm^3 g^{-1})	Mesopore ratio (%)	D_{HK} (nm)	D_{BJH} (nm)
W-ZSM-5	400	0.319	0.163	48.90	0.55	1.85
W-silicalite-1	351	0.298	0.176	40.94	0.55	2
ZSM-5	416	0.338	0.172	49.11	0.59	1.85
Silicalite-1	404	0.273	0.191	30.04	0.57	2.14

framework structure has a greater impact on the properties of the potential adsorption pores and channels by comparison.

3.2. CO_2 adsorption

Fig. 6 shows the adsorption isotherms of CO_2 on W-ZSM-5 and W-silicalite-1 at −15, 0, 25 and 50 °C at pressures up to 15 bar. The adsorption equilibrium curve is well consistent with the typical Langmuir isotherm, which is type I according to the IUPAC classification.[36] It should be pointed out that CO_2 enters the zeolite sample as a single layer in a reversible adsorption process, and this is a result of volume filling due to most of the space being microporous. The steric effect between the adsorbate and the pore structure of the adsorbent is negligible due to the sufficient pore volume. As the pressure reaches 15 bar, the isotherm shape becomes flat, indicating that the material is close to adsorption saturation. The measured maximum adsorption capacities of W-ZSM-5 and W-silicalite-1 are 81.69 and 69.96 cm^3 g^{-1}, respectively. For single layer adsorption, the difference in adsorption amount between the two samples is caused by the specific surface area and pore volume. Furthermore, although the CO_2 molecule is non-polar, it has a very large quadrupole and can be attracted by the electrostatic field in the zeolite. Therefore, the difference in the atoms causing the electronegativity in the zeolite framework also affects the number of adsorption sites. Adsorption decreases with increasing temperature due to the increase in the gas kinetic energy, which is determined by the physical adsorption characteristics. Since it is an exothermic process, heat rapidly accumulates as the adsorption process progresses, and thus high temperatures are unfavorable for the reaction.

In Fig. 6 and 7, the dashed lines represent the CO_2 adsorption data as fitted by the Toth model. In the process of designing an adsorption device, it is necessary to rely on an adsorption model to evaluate the adsorption properties of the adsorbent. The Toth model is actually a three-parameter improved Langmuir model, which has the advantage of accurately describing adsorption at high pressure, and is suitable for predicting the saturated adsorption capacity of the adsorbent. It assumes that the adsorption sites have a quasi-Gaussian distribution and that most of their adsorption energies are less than the peak adsorption energy. It is given by the following equation:[37–39]

$$q = \frac{q_m(bp)}{\left[1 + (bp)^t\right]^{1/t}} \quad (1)$$

$$t = t_0 + \alpha\left(1 + \frac{T_0}{T}\right) \quad (2)$$

where q is the equilibrium adsorbed amount at adsorbate gas pressure p, q_m is the maximum adsorbed amount, b is the Toth model adsorption constant, t is a constant representing the heterogeneity of the adsorbent, t_0 is the heterogeneity constant at the reference temperature T_0, T is the adsorption temperature and α describes the temperature dependence.

The CO_2 adsorption isotherm fitting parameters obtained from the Toth model are listed in Table 4, and the correlation coefficient R^2 is in a relatively high range of 0.9983–0.9998. With

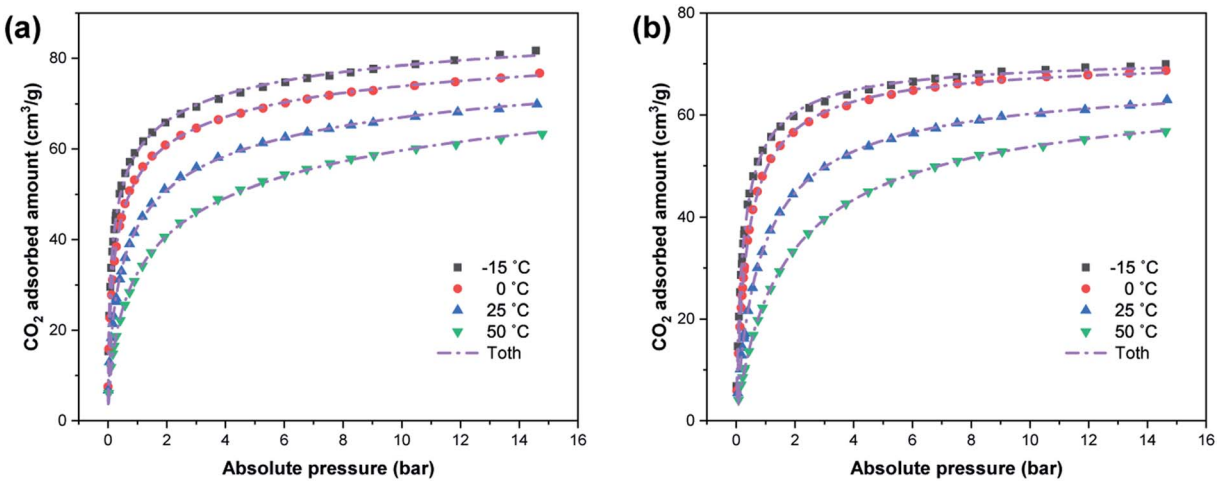

Fig. 6 Adsorption isotherms of CO_2 on (a) W-ZSM-5 and (b) W-silicalite-1 at different temperatures.

Table 4 Toth isotherm parameters for CO_2 adsorption at different temperatures

Sample	Temperature (°C)	q_m (cm^3 g^{-1})	b	t	R^2	$q_{15\ bar}$ (cm^3 g^{-1})
W-ZSM-5	−15	96.524	53.172	0.393	0.9984	80.79
	0	91.914	24.654	0.424	0.9983	76.39
	25	91.239	8.885	0.433	0.9984	70.22
	50	97.669	4.239	0.404	0.9988	63.89
W-silicalite-1	−15	72.038	5.679	0.787	0.9993	69.36
	0	71.670	3.370	0.824	0.9995	68.38
	25	68.618	1.451	0.817	0.9998	62.40
	50	68.216	0.717	0.795	0.9998	57.15
ZSM-5	0	89.481	11.322	0.482	0.9991	75.71
Silicalite-1	0	73.824	2.953	0.781	0.9994	69.21

the increase in temperature, the saturated adsorption amount on all adsorption sites on the adsorbent surface covered by adsorbate, represented by q_m, decreases, which is because the process is a physical adsorption process. b represents the activity coefficient of the competitive process between the solvent and the adsorbate that occupies the binding site on the solid surface. It can be seen from its value that the adsorbate has a higher thermodynamic activity coefficient in its bound state and free state at lower temperature. By calculation, the CO_2 adsorption amounts of the samples at 1 bar are up to 68–72% of those at 15 bar at 0 °C. However, this value becomes lower as the temperature rises, and it drops to 50% at 50 °C. Therefore, there is a larger amount of adsorption when the pressure exceeds atmospheric pressure, especially at high temperatures. t is further away from unity for W-ZSM-5 and ZSM-5 than W-silicalite-1 and silicalite-1, indicating that the

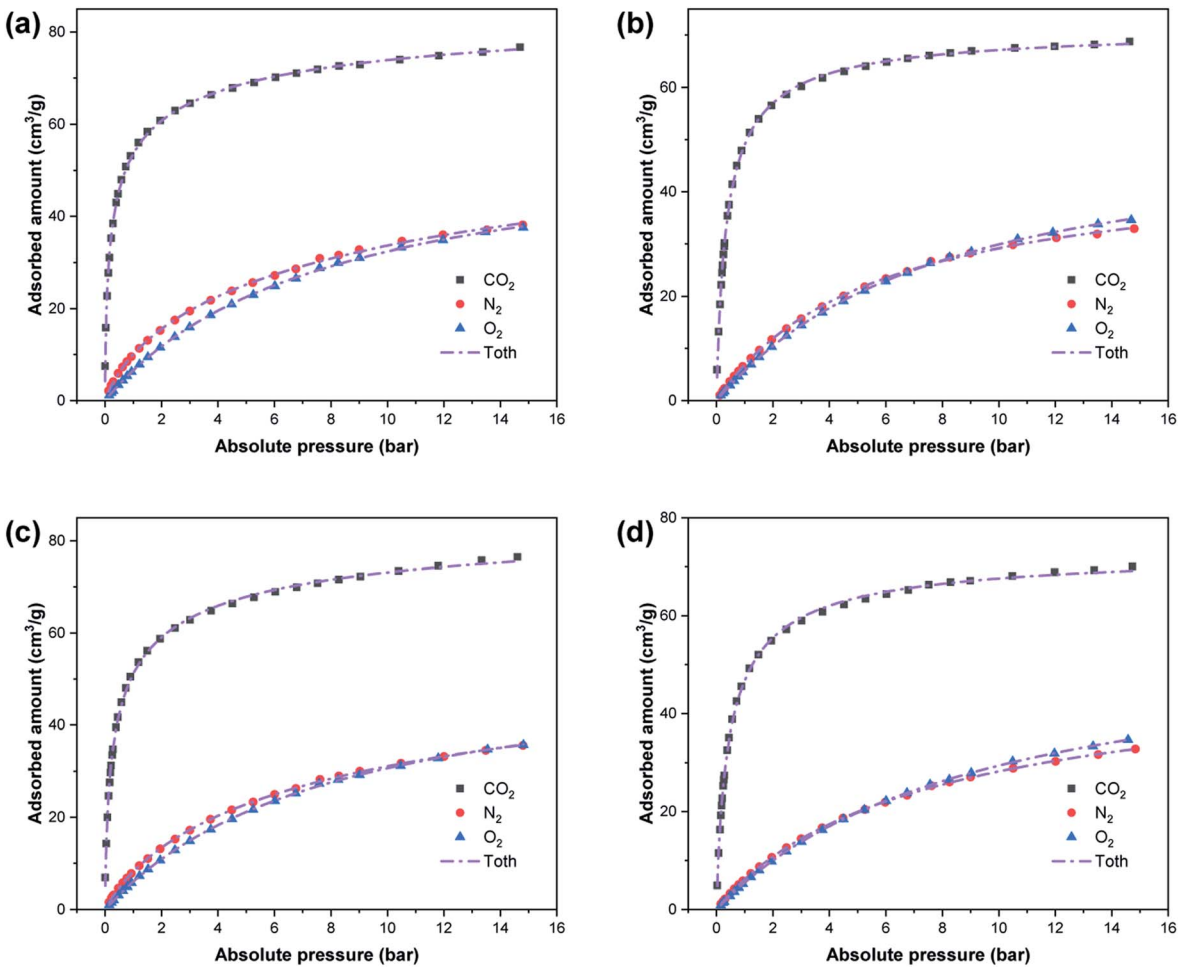

Fig. 7 Adsorption isotherms and Toth model fitting for CO_2, N_2 and O_2 on (a) W-ZSM-5, (b) W-silicalite-1, (c) ZSM-5 and (d) silicalite-1 at 0 °C.

Table 5 Toth isotherm parameters for N_2 and O_2 adsorption at 0 °C

Sample	Gas	q_m (cm^3 g^{-1})	b	t	R^2	$q_{15\ bar}$ (cm^3 g^{-1})
W-ZSM-5	N_2	77.195	0.262	0.555	0.9996	38.68
	O_2	58.385	0.128	0.986	0.9998	38.00
W-silicalite-1	N_2	45.918	0.176	0.996	0.9997	33.22
	O_2	51.022	0.122	1.101	0.9999	35.05
ZSM-5	N_2	62.738	0.195	0.695	0.9999	35.89
	O_2	54.106	0.123	1.041	0.9999	36.00
Silicalite-1	N_2	52.235	0.141	0.896	0.9999	32.92
	O_2	57.041	0.106	1.002	0.9999	35.07

adsorption systems of W-ZSM-5 and ZSM-5 are more heterogeneous.[40] The difference in the values of t can be explained by the fact that Al atoms have a greater effect on heterogeneity. The greater the heterogeneity of the adsorbent, the larger the CO_2 adsorption capacity achieved.

Fig. 7 shows a comparison of the CO_2, N_2, and O_2 adsorption equilibrium data for the four samples, and the Toth model fitting curves. The Toth isotherm fitting parameters for N_2 and O_2 are listed in Table 5, and R^2 is close to 1. Although CO_2, N_2 and O_2 are all non-polar molecules, the quadrupole moments of N_2 (1.2×10^{-26} esu cm^2) and O_2 (0.4×10^{-26} esu cm^2) are lower compared to that of CO_2 (4.3×10^{-26} esu cm^2).[41,42] The value of t for CO_2 is less than for N_2 and O_2, and that for O_2 is the largest. Thus, the adsorption amount of CO_2 is higher than that of N_2 and O_2, and this results in a selective adsorption performance.

The molar ratios of the adsorbed amounts of CO_2/N_2 and N_2/O_2 at 0.1, 1 and 15 bar are presented in Fig. 8. The adsorption selectivity for CO_2/N_2 and N_2/O_2 is determined by the following equation:

$$S = \frac{q_i/q_j}{p_i/p_j} \quad (3)$$

where S is the adsorption selectivity, q is the adsorption quantity (cm^3 g^{-1}) at partial pressure p (bar), and i and j represent CO_2, N_2 or O_2.

There is a wider pressure range in the Henry type isotherm for N_2 and O_2 compared to CO_2, and thus substantial selectivity is observed at less than 1 bar. The W and Al atoms in the framework have little effect on the selectivity at a high pressure of 15 bar, and mainly affect the selectivity in the low pressure region. The W-doped ZSM-5 exhibits reduced CO_2/N_2 selectivity and enhanced N_2/O_2 selectivity. The selectivity of the silicalite-1 type zeolite is hardly affected by the W-doping, so the selectivity difference is derived from the combined effects of W and Al atoms.

3.3. Water vapor adsorption

Fig. 9 shows the water vapor adsorption properties of the samples. It can be observed that all isotherms were linear and the adsorption process occurred in the Henry's law region due to the low temperature and saturated vapor pressure.[43] The H_2O adsorption amounts of W-silicalite-1 and silicalite-1 are relatively low, indicating that the presence or absence of Al largely determines the capacity for adsorbing water. The H_2O adsorption amounts of W-ZSM-5 and ZSM-5 are similar, and thus the doping with W has a greater influence on silicalite-1 in terms of absolute adsorption capacity. H_2O is a polar molecule, and the presence of the polarization energy causes its adsorption affinity to be several times that of CO_2.[44] As shown in Fig. 9(b), the CO_2/H_2O adsorption selectivity of W-ZSM-5 is slightly higher than that of ZSM-5, and that of W-silicalite-1 is three times that of silicalite-1. The flexible coordination state of tungsten prevents the formation of silanol, thereby reducing the number of H_2O adsorption sites.[45] In the framework without aluminum, tungsten plays an important role in preventing water vapor adsorption. This demonstrates that

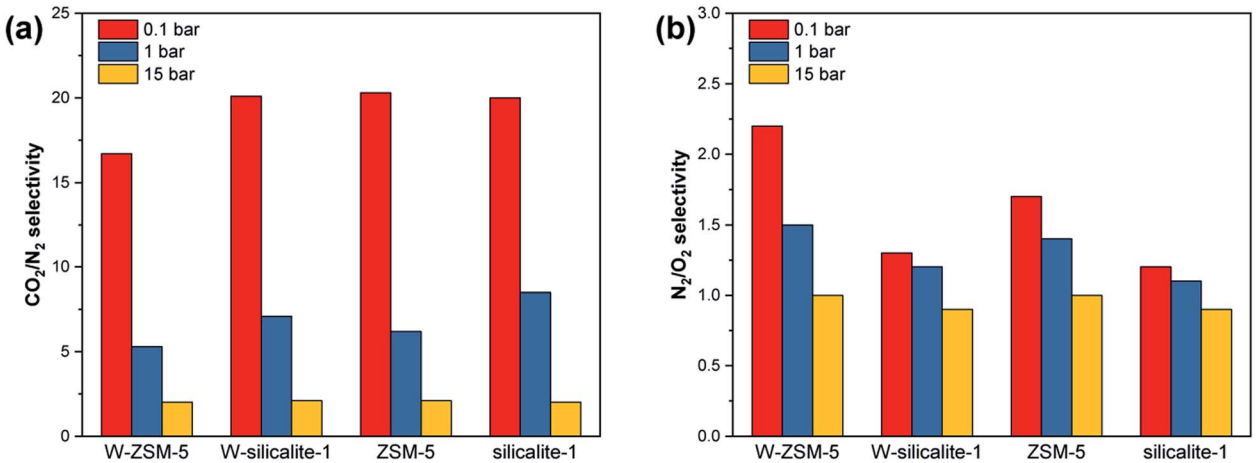

Fig. 8 Adsorption selectivity for (a) CO_2/N_2 and (b) N_2/O_2.

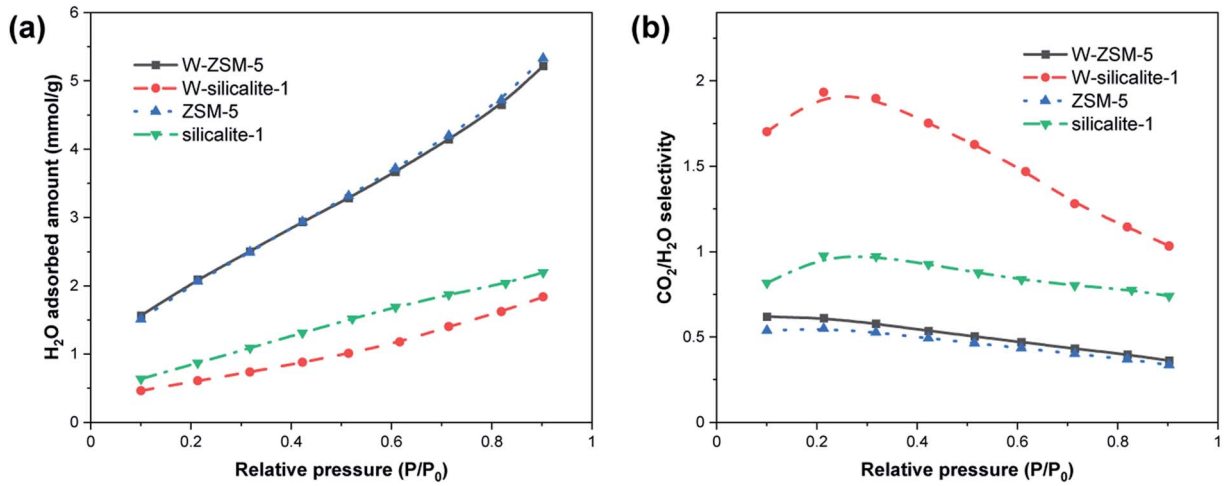

Fig. 9 H_2O vapor adsorption properties. (a) Isotherms at 25 °C and (b) selectivity for CO_2/H_2O.

under humid working conditions, the performance in adsorptive separation of CO_2 is improved due to the W-doping in the framework structures of ZSM-5 and silicalite-1.

4. Conclusions

In this work, framework hybrid zeolites with tungsten, W-ZSM-5/silicalite, were prepared from rice husk ash. The CO_2 and water vapor adsorption properties of the samples were explored, and then the CO_2/H_2O adsorption selectivity was evaluated. The characterization results show that the involvement of tungsten does not affect the crystal structure type of the zeolite, but prevents the formation of silanol and O–H groups. Through morphology and pore analyses, it is shown that tungsten has no effect on the appearance of the morphology, but the change in the framework leads to changes in the intrinsic specific surface area, pore volume and pore size distribution. The adsorption capacities of W-ZSM-5 and W-silicalite-1 are significantly improved, and the maximum capacities measured are 81.69 and 69.96 $cm^3\ g^{-1}$, respectively. The adsorption isotherms of CO_2, N_2 and O_2 are perfectly fitted by the Toth model. The flexible coordination state of tungsten prevents the formation of silanol, and this leads to the CO_2/H_2O selectivity of W-ZSM-5 being slightly higher than that of ZSM-5, and the CO_2/H_2O selectivity of W-silicalite-1 being three times that of silicalite-1. In summary, the framework hybrids W-ZSM-5/silicalite-1 are potential adsorbents for separating CO_2 under humid industrial conditions.

Conflicts of interest

The authors declare that they have no known competing financial interests or personal relationships that could have appeared to influence the work reported in this paper.

Acknowledgements

This work was funded by the National Natural Science Foundation of China (No. 51904073), the National Key Research and Development Project (No. 2019YFC1905200 and 2017YFB0304001), the Natural Science Foundation of Liaoning Province (No. 2020-BS-053), and the Postdoctoral Research Foundation of Northeastern University (No. 20190304).

References

1 M. Obersteiner, J. Bednar, F. Wagner, T. Gasser, P. Ciais, N. Forsell, S. Frank, P. Havlik, H. Valin, I. A. Janssens, *et al.*, How to spend a dwindling greenhouse gas budget, *Nat. Clim. Change*, 2018, **8**(1), 7.

2 D. Fang, X. Zhang, Q. Yu, T. C. Jin and L. Tian, A novel method for carbon dioxide emission forecasting based on improved Gaussian processes regression, *J. Cleaner Prod.*, 2018, **173**, 143–150.

3 G. Zhang, P. Zhao, Y. Xu, Z. Yang, H. Cheng and Y. Zhang, Structure property–CO_2 capture performance relations of amine-functionalized porous silica composite adsorbents, *ACS Appl. Mater. Interfaces*, 2018, **10**(40), 34340–34354.

4 A. A. Olajire, Recent progress on the nanoparticles-assisted greenhouse carbon dioxide conversion processes, *J. CO2 Util.*, 2018, **24**, 522–547.

5 IEA, *CO_2 emissions from fuel combustion 2018*, International Energy Agency, Paris, 2018.

6 F. E. Epiepang, J. Li, Y. Liu and R. T. Yang, Low-pressure performance evaluation of CO_2, H_2O and CH_4 on Li-LSX as a superior adsorbent for air prepurification, *Chem. Eng. Sci.*, 2016, **147**, 100–108.

7 F. Chen, Y. Wang, D. Bai, M. He, X. Gao and Y. He, Selective adsorption of C_2H_2 and CO_2 from CH_4 in an isoreticular series of MOFs constructed from unsymmetrical diisophthalate linkers and the effect of alkoxy group functionalization on gas adsorption, *J. Mater. Chem. A*, 2018, **6**(8), 3471–3478.

8 Y. Yang, C. Y. Chuah and T.-H. Bae, Polyamine-appended porous organic polymers for efficient post-combustion CO_2 capture, *Chem. Eng. J.*, 2019, **358**, 1227–1234.

9 A. M. Yousef, W. M. El-Maghlany, Y. A. Eldrainy and A. Attia, New approach for biogas purification using cryogenic separation and distillation process for CO_2 capture, *Energy*, 2018, **156**, 328–351.

10 F. Vega, M. Cano, S. Camino, B. Navarrete and J. Camino, Evaluation of the absorption performance of amine-based solvents for CO_2 capture based on partial oxy-combustion approach, *Int. J. Greenhouse Gas Control*, 2018, **73**, 95–103.

11 C.-P. Zhang, B. Li and Z.-G. Shao, First-principle investigation of CO and CO_2 adsorption on Fe-doped penta-graphene, *Appl. Surf. Sci.*, 2019, **469**, 641–646.

12 R. Castro-Muñoz, V. Fila, V. Martin-Gil and C. Muller, Enhanced CO_2 permeability in Matrimid (R) 5218 mixed matrix membranes for separating binary CO_2/CH_4 mixtures, *Sep. Purif. Technol.*, 2019, **210**, 553–562.

13 S. Xiang, Y. He, Z. Zhang, H. Wu, W. Zhou, R. Krishna and B. Chen, Microporous metal–organic framework with potential for carbon dioxide capture at ambient conditions, *Nat. Commun.*, 2012, **3**, 954–959.

14 J. Yan, Y. Li, H. Li, Y. Zhou, H. Xiao, B. Li and X. Ma, Effective removal of ruthenium(III) ions from wastewater by amidoxime modified zeolite X, *Microchem. J.*, 2019, **145**, 287–294.

15 D. K. Wanigarathna, B. Liu and J. Gao, Adsorption separation of R134a, R125, and R143a fluorocarbon mixtures using 13X and surface modified 5A zeolites, *AIChE J.*, 2018, **64**(2), 640–648.

16 A. Zukal, M. Shamzhy, M. Kubů and J. Čejka, The effect of pore size dimensions in isoreticular zeolites on carbon dioxide adsorption heats, *J. CO2 Util.*, 2018, **24**, 157–163.

17 N. Setthaya, P. Chindaprasirt, S. Yin and K. Pimraksa, TiO_2–zeolite photocatalysts made of metakaolin and rice husk ash for removal of methylene blue dye, *Powder Technol.*, 2017, **313**, 417–426.

18 R. Khoshbin and R. Karimzadeh, The beneficial use of ultrasound in free template synthesis of nanostructured ZSM-5 zeolite from rice husk ash used in catalytic cracking of light naphtha: effect of irradiation power, *Adv. Powder Technol.*, 2017, **28**(3), 973–982.

19 S. Jesudoss, J. J. Vijaya, K. Kaviyarasu, L. J. Kennedy, R. J. Ramalingam and H. A. Al-Lohedan, Anti-cancer activity of hierarchical ZSM-5 zeolites synthesized from rice-based waste materials, *RSC Adv.*, 2018, **8**(1), 481–490.

20 R. Pode, Potential applications of rice husk ash waste from rice husk biomass power plant, *Renewable Sustainable Energy Rev.*, 2016, **53**, 1468–1485.

21 J. Prasara-A and S. H. Gheewala, Sustainable utilization of rice husk ash from power plants: a review, *J. Cleaner Prod.*, 2017, **167**, 1020–1028.

22 H. Chen, Y. J. Zhang, P. Y. He and C. J. Li, Synthesis, characterization and modification of monolithic ZSM-5 from geopolymer for CO_2 capture: experiments and DFT calculations, *Energy*, 2019, **179**, 422–430.

23 P. J. Harlick and F. H. Tezel, An experimental adsorbent screening study for CO_2 removal from N_2, *Microporous Mesoporous Mater.*, 2004, **76**(1–3), 71–79.

24 Q. Liu, P. He, X. Qian, Z. Fei, Z. Zhang, X. Chen, J. Tang, M. Cui, X. Qiao and Y. Shi, Enhanced CO_2 adsorption performance on hierarchical porous ZSM-5 zeolite, *Energy Fuels*, 2017, **31**(12), 13933–13941.

25 A. Kalantarifard, A. Ghavaminejad and G. S. Yang, High CO_2 adsorption on improved ZSM-5 zeolite porous structure modified with ethylenediamine and desorption characteristics with microwave, *J. Mater. Cycles Waste Manage.*, 2017, **19**(1), 394–405.

26 Z. Lin, J. Wei, L. Geng, D. Mei and L. Liao, An amine double functionalized composite strategy for CO_2 adsorbent preparation using a ZSM-5/KIT-6 composite as a support, *Energy Technol.*, 2018, **6**(9), 1618–1626.

27 S. J. Datta, C. Khumnoon, Z. H. Lee, W. K. Moon, S. Docao, T. H. Nguyen, I. C. Hwang, D. Moon, P. Oleynikov, O. Terasaki, *et al.*, CO_2 capture from humid flue gases and humid atmosphere using a microporous coppersilicate, *Science*, 2015, **350**(6258), 302–306.

28 Q. Ke, T. Sun, X. Wei, Y. Guo and S. Wang, Enhanced trace carbon dioxide capture on heteroatom-substituted RHO zeolites under humid conditions, *ChemSusChem*, 2017, **10**(21), 4207–4214.

29 J. Ding, H. Xu, H. Wu and P. Wu, Liquid-phase oxidation of ethylamine to acetaldehyde oximes over tungsten-doped zeolites, *Sci. China: Chem.*, 2017, **60**(7), 942–949.

30 Y. Wang, T. Du, Z. Qiu, Y. Song, S. Che and X. Fang, CO_2 adsorption on polyethylenimine-modified ZSM-5 zeolite synthesized from rice husk ash, *Mater. Chem. Phys.*, 2018, **207**, 105–113.

31 Y. Liu, S. Han, D. Guan, S. Chen, Y. Wu, Y. Yang and N. Jiang, Rapid green synthesis of ZSM-5 zeolite from leached illite clay, *Microporous Mesoporous Mater.*, 2019, **280**, 324–330.

32 C. Zhang, Q. Wu, C. Lei, S. Pan, C. Bian, L. Wang, X. Meng and F.-S. Xiao, Solvent-free and mesoporogen-free synthesis of mesoporous aluminosilicate ZSM-5 zeolites with superior catalytic properties in the methanol-to-olefins reaction, *Ind. Eng. Chem. Res.*, 2017, **56**(6), 1450–1460.

33 Z. Lin, J. Wei, L. Geng, D. Mei and L. Liao, Adsorption of carbon dioxide by a novel amine impregnated ZSM-5/KIT-6 composite, *RSC Adv.*, 2017, **7**(86), 54422–54430.

34 I. O. Ali, A. M. Hassan, S. M. Shaaban and K. S. Soliman, Synthesis and characterization of ZSM-5 zeolite from rice husk ash and their adsorption of Pb^{2+} onto unmodified and surfactant-modified zeolite, *Sep. Purif. Technol.*, 2011, **83**, 38–44.

35 K. Barbera, F. Bonino, S. Bordiga, T. V. Janssens and P. Beato, Structure-deactivation relationship for ZSM-5 catalysts governed by framework defects, *J. Catal.*, 2011, **280**(2), 196–205.

36 Y. Gensterblum, A. Merkel, A. Busch and B. M. Krooss, High-pressure CH_4 and CO_2 sorption isotherms as a function of coal maturity and the influence of moisture, *Int. J. Coal Geol.*, 2013, **118**, 45–57.

37 V. Garshasbi, M. Jahangiri and M. Anbia, Equilibrium CO_2 adsorption on zeolite 13X prepared from natural clays, *Appl. Surf. Sci.*, 2017, **393**, 225–233.

38 H. Yi, Z. Wang, H. Liu, X. Tang, D. Ma, S. Zhao, B. Zhang, F. Gao and Y. Zuo, Adsorption of SO_2, NO, and CO_2 on activated carbons: equilibrium and thermodynamics, *J. Chem. Eng. Data*, 2014, **59**(5), 1556–1563.

39 D. P. Vargas, L. Giraldo and J. C. Moreno-Piraján, CO_2 adsorption on activated carbon honeycomb-monoliths: a comparison of Langmuir and Toth models, *Int. J. Mol. Sci.*, 2012, **13**(7), 8388–8397.

40 M. G. Plaza, I. Durán, N. Querejeta, F. Rubiera and C. Pevida, Experimental and simulation study of adsorption in postcombustion conditions using a microporous biochar. 1. CO_2 and N_2 adsorption, *Ind. Eng. Chem. Res.*, 2016, **55**(11), 3097–3112.

41 S. J. Chen, M. Zhu, Y. Fu, Y. X. Huang, Z. C. Tao and W. L. Li, Using 13X, LiX, and LiPdAgX zeolites for CO_2 capture from post-combustion flue gas, *Appl. Energy*, 2017, **191**, 87–98.

42 Y. Fu, Y. Liu, X. Yang, Z. Li, L. Jiang, C. Zhang, H. Wang and R. T. Yang, Thermodynamic analysis of molecular simulations of N_2 and O_2 adsorption on zeolites under plateau special conditions, *Appl. Surf. Sci.*, 2019, **480**, 868–875.

43 M. Pera-Titus, On an isotherm thermodynamically consistent in Henry's region for describing gas adsorption in microporous materials, *J. Colloid Interface Sci.*, 2010, **345**(2), 410–416.

44 T. D. Pham, Q. Liu and R. F. Lobo, Carbon dioxide and nitrogen adsorption on cation-exchanged SSZ-13 zeolites, *Langmuir*, 2013, **29**(2), 832–839.

45 J. Grand, S. N. Talapaneni, A. Vicente, C. Fernandez, E. Dib, H. A. Aleksandrov, G. N. Vayssilov, R. Retoux, P. Boullay, J.-P. Gilson, V. Valtchev and S. Mintova, One-pot synthesis of silanol-free nanosized MFI zeolite, *Nat. Mater.*, 2017, **16**(10), 1010–1015.

